Interpretation of High Frequency Ground Motion from Regional Seismic Network Observations

by Robert B. Herrmann and Luca Malagnini

Abstract. A procedure for modeling high frequency S-wave ground motion introduced by Yazd (1993) and used by Raoof et al (1999) and Malagnini et al (2002) is critically reviewed. The data analysis and interpretation are reviewed and synthetic seismograms are used to address several critical questions: the nature of ground motion distance scaling from the source to the first observation, the sensitivity of observed motion on focal mechanism, frequency content, component of motion and crustal structure.

This study suggests a strong relation between focal mechanism and the short hypocentral distance apparent geometrical and effective source radiation pattern term. Source depth has a strong effect on spectral content at frequencies less than 1.0 Hz. Because of the general departure from a r^{-1} geometrical spreading and the limited distance sampling in real data sets, absolute calibration of ground motion scaling for small earthquakes requires observations from $\mathbf{M}_W$ = 4.0 events whose moments have been determined from low-frequency waveform modeling.

Introduction

Digital recording of regional seismic network data became routine during the 1980's. Minicomputers in data centers digitized the analog data stream previously recorded on drum or photographic recorders. A reason for migrating to digital recording was to reduce cost through automation of event detection and location and the elimination of photographic recording. Although digital data were available, the limited dynamic range resulting from analog data acquisition and telemetry together with the 12-bit A/D permitted unclipped, resolvable recordings over a limited range of earthquake sizes. The economics of telemetry and emphasis on defining regional tectonics usually led to the choice of recording only vertical component motions.

In spite of the fact that these networks were not designed for high frequency ground motion studies of large earthquakes, many on-scale recordings of small earthquakes accumulated. Unknown site effects and the reliance upon vertical component data limited the use of these data for determining absolute source parameters even if the total instrument response were calibrated. Atkinson and Mereu (1992 - read paper) were among the first to use such data to understand ground motion scaling for engineering purposes.

Yazd (1993) realized that the observed ground motions were the result of the composite effects of the source, wave propagation from the source to the site, and local site effects. Also aware of the non-uniform geometrical spreading required by Atkinson and Mereu (1992), he developed a regression technique that emphasized the determination of

the propagation effects. His method has been extended and applied to different regions. Raoof et al (1999) applied the technique to 3-component broadband data in Southern California. Ortega (2003) studied wave propagation in central Mexico, Akinci et el (2001) in the Erzincan, Turkey region, Malagnini et al (2000b) in Germany, Malagnini et al (2000, 2000a, 2002) in various parts of Italy, Bay et al (2003) in Switzerland, Jeno (2000) in Utah and Jeon and Herrmann (2004) in Utah and Yellowstone.

As this technique was successively applied, several features were noted. The empirical amplitude-distance relation varies significantly from region to region, even at short distances from the source. The modeling of the regression results seems capable of describing absolute ground motions, which is important since the initial emphasis was on the distance dependence. Given the experience from these studies, it is timely to review the processing and modeling procedure and to consider the implications inherent assumptions on the forward modeling.

Data Processing

Data Preparation

Digital waveforms are acquired from the network. Each event may have 100 or more associated traces. Each trace is previewed to remove clipped or otherwise bad waveforms. The P- and S-times are picked, and the trace is corrected for instrument response to form a velocity time history in units of *m/sec*. The passband of the deconvolution is noted to define the range of acceptable frequencies for processing.

The traces are then bandpass filtered at a center frequency f_c by passing them through an 8-pole Butterworth high-pass filter with corner $f_c/\sqrt{2}$ followed by an 8-pole low-pass filter with corner $\sqrt{2}\, f_c$ and the combined peak filter response is adjusted to be 1.0. The following parameters are derived from the filtered traces and tabulated for later processing:

- peak filtered velocity (*m/sec*) following the S arrival,
- the signal duration, defined as the interval within which the integral of filtered velocity squared following the S arrival changes from 5% to 75% of the maximum (Raoof et al 1999 ; Bay et al 2003);
- the RMS Fourier velocity spectra (*m*) of the waveform within the duration window between frequencies $f_c/\sqrt{2}$ and $\sqrt{2}\, f_c$,
- the random vibration theory (RVT) estimate of the peak filtered velocity with 5% and 95% bounds (Cartwright and Longuet-Higgins, 1956) obtained using the measured signal duration and the actual filtered velocity spectrum of the signal within that window,
- RMS signal level as a function of time for coda-Q analysis and signal-to-noise estimation, and
- event and station identification

The purpose of the extensive tabulation is to preserve enough information to characterize the signal for later analysis. The use of such narrow band filters rather than the traditional damped single degree of freedom oscillator used for response spectra requires comment. Although the typical 5% damped oscillator appears to be a sharp filter, it is

not. Its output waveform depends upon the duration and frequency content of the input signal. If the frequency content of the signal is significantly greater than the filter frequency, the signal is affected by the smooth part of the transfer function. The filtering of other signals may be strongly affected by the oscillator resonance. The net effect is that the frequency content of the resultant signal is highly dependent on the specific nature of the signal. On the other hand, the narrow band combination of Butterworth filters used here will yield a filtered signal with frequency content close to the center frequency of the filter. Thus we are better able to characterize the propagation of one particular frequency component of the ground motion. Although the combination of Butterworth filters better predicts the frequency content, to avoid working with an imprecise value for the frequency content of the filtered waveform, we will subsequently define a forward model that is constrained by synthetic motions passed through the same filters. The other difficulty with the use of lightly damped oscillators as filters is that the scaling from small earthquake observations to large earthquake motions is non-linear because of the interplay of signal duration, signal frequency content and the oscillator frequency in estimating peak-motions. This is less of a problem with the use of the narrow bandpass filters.

The objective of the data processing is the construction of a forward model that can be used with RVT to predict the observed filtered velocities, but which will also be able to predict response spectra or peak ground motions (Boore, 2003). To do this, only the Fourier spectra and the duration of the motion are required. These are the measurements that form the basis of the Atkinson and Boore (1995) model for eastern North America, who then used RVT to predict response spectra and peak motions. We analyze and model *both* the Fourier velocity *and* the peak filtered velocity values. Our reason for this extra effort is that this recognizes the imperfections in both the data and the modeling process. The observed Fourier velocity spectra requires a determination of the duration, which we have found to show a lot of scatter; the observed filtered peak velocity values have no such uncertainty. RVT modeling of the peak filtered velocities, though, requires the duration value. Our forward model must be consistent with the three sets of observations, Fourier spectra, peak motion and duration, in the context of RVT modeling before we are satisfied that we have constructed an internally self-consistent model.

Observed Motions

The observed ground motion is a function of source, site and path. Unless non-linear ground motions occur at the site, these three factors are theoretically separable, and additive in a logarithmic sense. Thus the observed logarithm of the measured ground motion, $A(r, f)$, either filtered peak or Fourier velocity, can be written as

$$A_{jk}(r, f) = E_j(r_{ref}, f) + S_k(f) + D(r, f), \qquad (1)$$

where r is the hypocentral distance, f is the observed frequency, j is the source index, $1 \le j \le J$, k is the site index, $1 \le k \le K$, r_{ref} is a reference distance, and E, S and D are the excitation, site and distance functions.

The term excitation is used since the regression defines the scaling of observed ground motions and says nothing about the seismic source. Other studies, such as Atkinson and Silva (1997), define a Fourier acceleration spectrum at a reference distance of 1 km. To emphasize that we wish to stably characterize observations, we specifically note the use of a reference distance by the term r_{ref}. The reference distance r_{ref} is selected to

be within the range of observed distances so that we interpolate within the data set rather than extrapolate beyond, to be far enough from the source that errors in source depth do not significantly affect hypocentral distance, and yet not so far that expected super-critically reflected crustal arrivals complicate the motion. For these reasons we often use a reference distance of $r_{ref} = 40$ km for our studies. It is hoped that simple wave propagation models will suffice to predict the $A_{jk}(f, r_{ref})$. Of course, there must be observations on both sides of this reference distance to avoid extrapolation of poor data sets.

The function $D(r)$ in (1) is approximated by piecewise linear segments with a condition of continuity. This interpolation function is often discussed in finite element texts (Huebner, 1974) and was used for ground motion scaling by Anderson and Lei (1994), Savage and Anderson (1995) and Harmsen (1997). Using this interpolation function, the $D(r)$ is described in terms of the values at L nodes as

$$D(r) = \sum_{l=1}^{L} D_l N_l(r).$$

The linear interpolation function, the $N_l(r)$ is non-zero in the range $r_l \le r \le r_{l+1}$ and $D(r_l) = D_l$ by definition. The choice of the nodes is made by examining the distribution of data with distance. Nodes are spaced to enclose a sufficient number of observations for a stable, smooth inversion.

By construction (1) forms a linear minimization problem in $J + K + L$ unknowns. However, it is singular unless constrained. The constraints used here are

a) $D(r_{ref}) = 0$, where $r_{ref} = 40$ km,

b) $\sum_k S_k(f) = 0$, and

c) $D(r)$ is smooth.

Constraints are added to the system of linear equations by adding additional rows in the linear algebra problem; these rows are heavily weighted. Anderson and Lei (1994) and Harmsen (1997) use a linearity constraint on $D(r)$ by requiring the numerical second derivative estimate to be zero. This is important if it is necessary to pass an acceptable distance function through a gap in distances. We apply the condition

$$D_{l-1} - 2D_l + D_{l+1} = 0.$$

Strictly speaking, this condition is only a linearity constraint if the r_l are evenly spaced. We use an unequal spacing to ensure a sufficient number of observations to define the distance function within a given data range and to permit greater sampling in regions of expected rapid change distance function. For unevenly spaced data, this condition is a linearity constraint in a mapped distance space.

The site constraint b) is one of many possible. One could force hard rock sites to have individual site terms of zero. The site constraint used here focuses on relative site effects, and has the consequence that common site effects are then mapped into the $E_j(r_{ref})$ term, which is another reason that we refer to this symbol as an excitation of observed data rather than as an absolute source term. The $E_j(r_{ref})$ are now seen to represent an expected ground motion level at a distance of r_{ref} from the source. When three-component data are available, the site constraint can be modified to apply to the vertical

or to the horizontal components only, with the other component floating freely to permit the determination of the site H/Z ratios, for example.

Other aspects of this regression model, related to trade-offs between the excitation, site and distance terms, must be understood before accepting the results of the inversion. Two extreme examples illustrate the problems. If only one event appears in a specific distance range, then there will be a trade-off between the excitation for that event and the adjacent distance terms. This occurs if an event is separated by a distance of the network dimensions from a neighboring event or if the distribution of distance nodes is too dense. As another extreme example, if only one station appears in a narrow range of distances and if it has an anomalous response, then the $D(r)$ will be distorted by this station and a bias introduced in all other site terms because of constraint b).

In practice plotting the observation distances by event and by station is a good diagnostic for discarding events and defining the distance nodes. The goal is that each station observe events over a wide range of distances overlapping those of other stations, and that the distance ranges of events overlap.

The regression is applied at each processed frequency to yield the $E_j(r_{ref}, f)$, $S_k(f)$ and $D(r_{jk}, f)$ for the Fourier velocity and for the peak filtered velocity. The next step is to interpret these observations in terms of a predictive model.

Data Modeling

Theoretical Fourier Velocity Spectra

The predicted Fourier velocity spectra , $a(r, f)$, at a frequency f and a hypocentral distance r is modeled as

$$a(r, f) = s(f, \mathbf{M}_W) g(r) e^{-\pi f r / Q(f) \beta} V(f) e^{-\pi f \kappa} . \qquad (2)$$

where $s(f, \mathbf{M}_W)$ is the source excitation as a function of moment-magnitude, $g(r)$ is the geometrical spreading function, $Q(f)$ is the frequency dependent quality factor written as $Q_0(f/1.0)^{\eta}$, Q_0 is the quality factor at 1.0 Hz, $V(f)$ is a frequency dependent site amplification, and κ controls site dependent attenuation of high frequency (Anderson and Hough, 1984).

Following Boore (2003), a typical expression for $s(f, \mathbf{M}_W)$, the Fourier velocity spectra at a distance of 1000 m from the source, is

$$s(f, M_W) = K \frac{M_0}{4\pi\rho\beta^3 1000} (2\pi f) S(f) \qquad (3)$$

where $\log M_0(nt \cdot m) = 1.5 M_W + 9.05$ (Hanks and Kanamori, 1979), $\rho\,(kg \cdot m^{-3})$ is the material density at the source, $\beta(m/s)$ is the shear-wave velocity at the source, $S(f)$ is the omega-square displacement spectrum source model

$$S(f) = \frac{1}{1 + (f/f_c)^2} .$$

Following Brune (1970, 1971), f_c is defined in terms of the shear wave velocity at the source, $\beta\,(m/s)$, the seismic moment, $\log M_0(nt \cdot m)$ and the stress parameter, $\Delta\sigma\,(MPa)$, by

$$f_c = 49 \beta (\Delta\sigma / M_0)^{1/3} .$$

and the constant K includes the composite factors of the radiation pattern, free-surface amplification and the partition of the initial shear-wave amplitude into the recorded component. We use the constant K and do not try to define the separate effects. The units of the velocity spectra $s(f, M_W)$ is m. The geometrical spreading function $g(r)$ in (2) is dimensionless since it gives the diminution of amplitude relative to $r = 1000m$.

A comparison of the regression parameters for the velocity spectra to the terms of this formula shows the association:

$$10^E = s(f, \mathbf{M}_W) g(r_{ref}) e^{-\pi f r_{ref}/Q(f)\beta} \overline{V(f) e^{-\pi f \kappa}} \tag{3}$$

$$10^D = \frac{g(r) e^{-\pi f r/Q(f)\beta}}{g(r_{ref}) e^{-\pi f r_{ref}/Q(f)\beta}} \tag{4}$$

$$10^{S_i} = \frac{V(f) e^{-\pi f \kappa}}{\overline{V(f) e^{-\pi f \kappa}}}\,, \tag{5}$$

where $\overline{V(f) e^{-\pi \kappa f}}$ is the network average site effect arising from constraint b).

Time domain modeling

RVT requires the signal duration in addition to the predicted signal spectra at the site. We have found much scatter in our duration estimates because the observed signals are superimposed on ground noise and because we use an automatic procedure to determine it from each trace. This is ameliorated by binning the durations according to distance, determining the median within each bin and then fitting the median values using the same linear interpolation scheme used for distance:

$$T(r) = \sum_{l=1}^{L} T_l N_l(r),$$

but with the single constraint is that $T(r = 0 \text{ km}) = 0$ since we assume that the duration of small earthquakes is small at short distances. We bin the observed durations to obtain an L1 median and then use an L2-norm to find a smooth duration relation from the median values.

The RVT duration, which depends on the source duration and a propagation terms, is written as

$$T_S + T(r)\,,$$

where T_S is the source contribution and $T(r)$ is the distance dependent wave propagation contribution to total duration.

By studying small earthquakes, we can assume that the measured durations are essentially the $T(r)$ since the T_S is assumed to be small. Because of this the $r = 0$ constraint is acceptable. Forward predictions will always include the T_S term which is often assumed to be proportional to $1/f_c$ (Boore, 2003).

Modeling

We use the following sequence to model the observables of (1).

1. Fit the Fourier velocity $D(r)$ in terms of $g(r)$ and $Q(f)$. We assume that the $Q(f)$ is independent of distance. Even with our typical range of filter frequencies between 1 and 16 Hz, the $e^{-\pi fr/Q(f)\beta}$ trades off with the $g(r)$ so that we cannot uniquely determine either. We assume that the 1 Hz $D(r)$ is not strongly affected by the $Q(f)$ and use this as a guide to the choice of $g(r)$. The $g(r)$ is kept as simple as possible, e.g., with just a few nodes between 1 and 400 km. The variation of the $D(r)$ as a function of frequency at large distance is indicative of the value of η - there will be a large spread for small η and no spread for $\eta = 1$. It is not difficult to find an acceptable set of parameters.

2. Test this $g(r)$ and $Q(f)$ choice and refine the $T(r)$ values by fitting the $D(r)$ for the filtered peak velocity. To do this, we assume a small $\mathbf{M}_W$, e.g., 3.0, for the event size to predict the $s(f, \mathbf{M}_W)$. Even though the source term will not divide out for the normalized $D(r)$ in the way that it did for the Fourier velocity spectra to yield (4), we assume that the sensitivity to the source effect is effectively removed when using at narrow bandpass filtered signals. The purpose of this step is to check the internal consistency of the $g(r)$, $Q(f)$ and $T(r)$ to explain both the distance dependence of the Fourier velocity and the peak filtered motions.

3. Constrain the $\overline{V(f)e^{-\pi\kappa f}}$ term. Figure 1 shows the Fourier acceleration spectra at a distance of 1 km for 4 different moment magnitudes and two stress drops, 1 and 30 MPa for $\beta = 3500\, m/s$, $\rho = 2800\, kg/m^3$ and $K = 1$. We see that the stress drop barely affects the source spectra in the 1-16 Hz frequency band for the smallest event. As the seismic moment increases, source spectra is insensitive to the stress drop only at the lower frequencies. Lacking detailed information about the moment magnitudes of these small events and the mean site specific $V(f)$, we presently use the parameter κ_{eff} in our modeling, where

$$e^{-\pi\kappa_{eff} f} \approx \overline{V(f)e^{-\pi\kappa f}}\,.$$

   This may seem odd mathematically, but since the $V(f)$ generally increases from 1.0 at low frequency to a fixed high frequency value and there is only a limited frequency range to fit a logarithmic function, we assume that this approximation is in error by only a constant factor at most, which could be included in the K constant.

Synthetic Seismogram Studies

Although the data modeling procedure can adequately characterize the regression results in a manner that interpolates between the observations, it is only a mathematical exercise in parameterization unless some fundamental questions concerning data interpretation are addressed. This must be done before one can use these results for a prediction of absolute ground motion. Important questions that must be addressed are as follow:

- Is a study of vertical component motions useful for predicting horizontal motions?
- What is the nature of the ground motion scaling from the source to the first observation distance? Does this depend upon the focal mechanism?
- How does crustal structure affect ground motions, especially at larger distances?
- Does the simple forward prediction model apply to all frequencies?

The first question arises because of the abundance of vertical component observations, especially in areas of low to moderate seismicity. The immediate necessity of

defining ground motion scaling relations may not permit waiting until there is an adequate three component data set. In addition, the use of older data gets additional results from the previous seismic network recordings.

The second question acknowledges the fact that the prediction of ground motions outside the range of observations, either in terms of distance or source size, is an exercise in extrapolation subject to underlying assumptions. This caution also applies to the inverse process of estimating earthquake source parameters since the extrapolation of the observations back to the source requires an assumption of the geometrical spreading at short distances.

Ground motions at epicentral distances greater than 100 km can cause significant damage even in regions of high attenuation. Since these motions will be influenced by signals returned from deeper crustal layers (Burger et al, 1987), the effect of deeper crustal structure must be appreciated to understand regional variations in ground motion scaling.

To address these issues, a suite of complete wavenumber integration synthetic seismograms were generated (Herrmann, 2003CPS). The seismogram motions following the S-arrival were processed and interpreted as described in the Data Processing and Modeling sections.

The Network and Events. The seismic network consists of 22 stations distributed uniformly over an approximately 440 x 440 km region. Within this region 240 earthquakes are randomly distributed, with 40 confined near the center of the region to ensure sufficient observations at short distance. The events and stations are shown in Figure 2. This configuration was chosen since its size is comparable to the coverage of some regional seismic networks and since this configuration would provide data coverage to distances to 500 km. The smallest hypocentral distance is limited by the shallowest focal depth and the shortest epicentral distance.

Earth Models. Green's functions were computed for three source depths and six velocity models. The source depths were 5, 10 and 15 km. The source depths were chosen to typical of crustal earthquakes with the 1:2:1 as the relative ratio of the number of earthquakes at each depth. Three of the models are perturbations on the Central U.S. model (Herrmann and Ammon, 1997), denoted as HCUS. This model consists of a 4-layer 40 km thick crust overlying a halfspace. The TCUS and MCUS models have 32 and 48 km thick crusts, respectively, obtained by changing the thickness of the lower crustal layer. The ECUS model has a 0.6 km thick low velocity sediment section on top of the HCUS model as an approximation to the Mississippi Embayment near New Madrid, Missouri. Finally the MHAM model, derived to fit a broadband waveform of the September 26, 1990 Hamburg, Missouri, earthquake (Herrmann and Ammon, 1997) has many more layers and is characterized by a transitional, rather than a sharp Moho. We note that the P-wave first arrival times of the MHAM and MCUS models are essentially the same for a surface-focus event and distances of 0 - 300 km. The final model, NWIT, has a lower velocity upper crust and may be appropriate for northwest Italy. The shear-wave velocity models are compared in Figure 3.

The models also had a causal Q_S. The TCUS, HCUS, MCUS and MHAM models has $Q_S = 100$ in the top 1 kilometer and $Q_S = 1000$ in the remainder of the model. The ECUS model had $Q_S =$ in the upper 600 meters, 100 in the next kilometer and 1000 in the

rest of the model. The NWIT model has a uniform $Q_S = 250$ in the entire model.

Regional Tectonics. To test the effect of focal mechanism, three sets of synthetic seismograms were computed for each velocity model: SS - all 240 events consisted of a north striking vertical strike-slip mechanism; 45 - all 240 events consisted of a north striking 45 degree dip-slip mechanism; MX - a random 50-50 mixture of vertical strike-slip and 45 degree dip-slip mechanisms. These three different environments are observed, e.g., the dip-slip mechanism predominates in southeastern Canada and the northeastern United States (Du et al 2003), the mixture in the New Madrid region (Herrmann and Ammon, 1997), and the strike-slip in parts of California. The uniform northerly strike used is acceptable because the station distribution adequately samples the radiation patterns from the sources and we are interested in network averaged estimates of ground motion. The synthetics are point source synthetics - no directivity effect is included in the simulations and thus no distinction whether the 45 source is a normal or thrust fault. The source time function is the parabolic pulse of Herrmann (1979) which has a duration of 0.4 sec. The pulse spectrum has zeros at 5.0 Hz and the Nyquist frequency of 10.0 Hz to ensure simple finite pulse at short distances. An analysis of high frequencies was not attempted because of the simplicity of the velocity models.

Synthetic Data Sets. The data sets consist of combinations of the 6 models and 3 focal mechanism types with 5696 three-component seismograms (vertical, north-south and east-west) for each of the 18 data sets. The ground motion data sets for regression consisted of the 5696 vertical component motions (Z), 11392 horizontal motions (H) and the 17088 three component motions (A). The constraints on the site terms were that $\sum S_Z = 0$ for the Z and A cases, and $\sum S_H = 0$ for the H case. The north-south and east-west waveforms are combinations of P-SV and SH waves.

Each data set was processed with filter center frequencies of 0.25, 0.33, 0.50, 1.0, 2.0, 3.0 and 4.0 Hz, with the upper frequency limit controlled by the 10 Hz Nyquist frequency of the synthetics.

Regression Results

Focal mechanism effect.

For this comparison we restrict ourselves to the HCUS model. Figure 4 presents the regression $D(r)$ in a manner that emphasizes departure from $1/r$ spreading, where r is the hypocentral distance. The solid and dashed curves represent the regression on the different components of motion. The filter frequency is 1.0 Hz, which should emphasize the high-frequency S-wave arrivals and not the low frequency surface wave arrivals. In addition, the filter frequency is high enough that the filtered P-wave wave should not overlap the S-wave signal at distances at short as 10 km, which is one reason that hypocentral distances less than 10 km were not considered in the analysis.

Focusing first at distances less than 40 km, we note the following. First, the $D(r)$ for the peak filtered velocity indicates a slightly more rapid decrease of amplitude with distance than the Fourier velocity. This can be understood from random vibration theory as the consequence of duration increasing with distance. A more important observation is that while the $D(r)$ for horizontal motion are similar for all mechanisms, exhibiting a spreading slightly greater than $1/r$, the data sets consisting solely of vertical component motion (Z), or including vertical component motion (A), have a stronger dependence upon focal

mechanism. The consequence of this observation is that one must be careful in treating vertical component data sets as a substitute for horizontal component observations. In addition, the H/Z ratio can change with distance which calls into question the regression constraint that the site term is independent of distance.

At larger distances, the effect of focal mechanism is again strongly seen in the vertical component motion, with differences of about a factor of 2 at 160 km for the SS and 45 motions. This is understandable from source models - the takeoff angle associated with the supercritical reflections from the Moho is near the maximum SV radiation on the focal sphere for the 45 degree dip-slip mechanism. The SV generation affects the radial component motion, but the effect is averaged when the radial and transverse ground motion components are combined. It is interesting that the ground motions for the strike-slip environment are closer to $1/r$ spreading at short distances than for the 45 degree dip-slip mechanism. The horizontal motion (H) is the least sensitive to mechanism.

Crustal structure

The effect of crustal thickness is shown in Figure 5 by comparing the regression results for the 32 km, 40 km and 48 km thick crustal models. Since just the lower crust is changed, few differences are seen at short distances, for which the S-wave arrivals are due to signals propagating upward from the source. At larger distances, the large Moho signal contribution moves to larger distances as the total crustal thickness increases.

Figure 6 compares the MCUS and MHAM models. As mentioned earlier, these have similar surface-focus P-wave first arrival times to 300 km. We see that the corresponding $D(r)$ are similar, which indicates that the gross properties of the distance dependence of ground motion do not depend upon the fine details of the crustal model. We again note that the SS distance dependence is much closer to $1/R$ than for the 45 data set.

Figure 7 considers the effects of a thick low-velocity sediment cap on the HCUS model. The interesting result is that although the focal mechanism related effects at short distance continue, the differences between the regressions on the vertical and horizontal components of ground motion significantly reduced sufficiently that the vertical component results may be used for the horizontal.

Finally, the $D(r)$ for the HCUS and the significantly different NWIT models are compared in Figure 8. We again see difference between the two focal mechanism data sets, but that the variation among the Z, H and A data sets is generally reduced. The difference in the values of the $D(r)$ at large distances is due to the lower Q's used for the NWIT crust.

Frequency content and fit.

The Fourier velocity and filtered time-domain peak velocity $D(r)$ are compared in Figure 9, for the 45 data set of the HCUS model at frequencies of 0.25, 1.0 and 4.0 Hz. While we see that the 1.0 and 4.0 Hz $D(r)$ are similar, except for a slight Q effect at large distance, these are very different from the 0.25 Hz results. We attribute this to the fact that

the high frequencies data set consists of individual S-wave arrivals while the low frequency data sets consist of coherent surface-wave arrivals. The 0.25 Hz frequency domain $D(r)$ can be characterized by a $r^{-1/2}$ geometrical spreading over its entire range. The corresponding time domain regression at 0.25 Hz shows a slightly greater distance dependence because of increasing duration with distance.

The regression (1) also provides the residual of fit. We examined the distribution of residuals of fit to all data sets, the standard deviation of the data varied from about 0.06 to 0.35 $\log_{10}$ units with a suggestion of an increase with increasing frequency. The mean of the 756 individual standard deviations is 0.202, a number which is similar to that seen in real data sets (Malagnini etc). This variability in fitting the synthetics is attributed to the different sampling of the focal sphere by the different rays forming each observed signal which may also be a contributor to the lack of fit to actual data, which are also affected by scattering and other wave propagation phenomena.

Duration

The measured durations exhibit scatter but also a dependence upon frequency and velocity model. Figure 10 compares the HCUS and NWIT model durations for all components for the 45 source. We observed that the durations at frequencies less than 1.0 Hz generally increase with distance more rapidly than for higher frequencies. We see that the 1.0 Hz durations generally increase with distance for the NWIT model, but those for the HCUS and the other near constant upper crustal models, seem to flatten after an initial rise. A monotonic increase of duration would be expected for a surface-wave packet, but a constant duration is expected if the peak S-wave motion is controlled by just a few distinct arrivals. The increased scatter at low frequencies is obvious as is the difficulty in defining a $T(r)$ relation because of the scatter. In a study of three-component ground motion in Southern California, Raoof *et al* (1999) observed the measured duration at frequencies 1.0 Hz and greater were very similar and that the lower frequencies had greater duration.

Excitation

For each of the 54 regression data sets, an $E(f)$ is estimated. Figure 11 presents the results for the HCUS model and SS mechanism. The scatter at high frequencies can be attributed to different sampling of the source radiation pattern by the network - recall that not all events are surrounded by a uniform azimuthal station coverage. The most significant feature of these plots appears at frequencies less than 1.0 Hz, for which the excitation splits into three different populations with the 5.0 km source depth having significantly higher levels at a frequency of 0.25 Hz. This is due to the fact that the low frequency motions, especially on the vertical component, contain the contributions not only of the S-wave field but also the Rayleigh-wave fundamental mode, whose excitation is mechanism and source depth dependent. This depth dependence at lower frequencies would lead to increased variability in the mean E level at 0.25 Hz compared to higher frequencies. We also note that data from shallow sources might cause us to attribute the observed shapes to the source spectrum instead of to the depth.

For TCUS, HCUS, MCUS and MHAM velocity models, we noted that the Fourier velocity $E(40\,km)$ have very similar levels irrespective of the mechanism and component of motion in spite of the larger differences in the apparent distance spreading. The fortuitous choice of a 40 km reference distance for these focal mechanisms means that the aggregate of rays from the source to this distance sample similar radiation patterns. This observation, together with the very different geometrical spreading at short distances implies a very strong relation between the radiation pattern effects and the geometrical spreading at short distance to yield the similar levels at a distance of 40 km. Boore and Boatwright (1984) noted that the average source radiation pattern depended upon the take-off angle for local, regional and teleseismic signals. Our study provides more detail upon how the change in effective radiation pattern from short to larger distances expresses itself in an additional distance dependence.

Figure 11 also presents the predicted $E(40\,km)$ for the HCUS model. The regression $D(r)$ were analyzed in the manner described in Step 1. The $g(r)$ at distances less than 40 km for the SS data set was $r^{-1.1}$, $r^{-1.3}$ and $r^{-1.0}$ for the (A), (H) and (Z) data sets respectively. To fit the mean $E(40\,km)$ shown in Figure 11, $K = 0.4$, 0.78 and 0.24, were used respectively. A similar fit to the 45 mechanism required $g(r) = r^{-1.5}$ and $K = 1.6$ for the (A), $g(r) = r^{-1.3}$ and $K = 0.78$ for the (H), and $g(r) = r^{-1.7}$ and $K = 4.0$ for the (Z) data sets.

The RVT prediction of the peak filtered amplitudes underpredict the regression $E(40\,km)$ in Figure 11. We attribute this to the subtle differences of attempting to predict the coherent pulse amplitude using RVT.

Discussion

The significant result of this work is that we note a strong relationship between the geometrical spreading, $g(r)$ and the K term of (3) in order to yield the $E(40\,km)$, seemingly independent of source or component. The interdependence is not surprising since at these short distances the dependence of average radiation pattern change with take-off angle maps into an apparent distance dependence that is in addition to the wave propagation $1/r$. The K constant in (3) represents the combined effects of the three factors of radiation pattern, free-surface effect and partition of shear-wave motion into the observed component (Boore, 2003). Rather than using a preset set of values for the K as is typically done using the Boore (1983, 2003) model, we must calibrate the K to the specific data set to permit absolute ground motion prediction. The source spectra plots of Figure 1 suggest that this calibration can be done by adjusting the K value for the observed $g(r)$ to match the observed E at frequencies less than 2.0 Hz for $\mathbf{M}_w = 4$ events. These moment magnitudes must be determined independently of assumptions of short distance radiation pattern and geometrical spreading, which is possible by modeling the long period waveforms or surface-wave spectra. We suggest a fourth step to the data modeling:

4. Calibrate the absolute scaling by determining the source K that matches the low frequency components of the excitation for the regression estimate of the $g(r)$. For an $\mathbf{M}_W = 4.0$ earthquake, this would mean fitting frequencies less than 2.0 Hz. The $\mathbf{M}_W$ must be estimated independently of this regression.

The expected difference between short-distance scaling for the SS and 45 environments, will have implications for probabilistic seismic hazard analysis. Because of the observation of similar levels at 40 km, we expect larger motions near the source for the 45 degree dip-slip environment than for the strike-slip environment. This would map into larger expected hazard near faults in the 45 degree dip-slip environment.

Because of the regression results, we are more comfortable with using a geometrical spreading faster than r^{-1}, especially if we know that we are not in a strike-slip environment.

To answer the questions posed in this study, we conclude that a study of vertical motions may be useful for predicting horizontal motions (ECUS and NWIT models), that local crustal structure is important for understanding motions at all distances and for defining the $E(40\,km)$, that typical regional focal mechanism is reflected in the short distance scaling. The distance dependence may be different above and below 1.0 Hz.

The study of small earthquakes permits a robust empirical determination of the distance of high frequency ground motion. The forward model can be considered an estimate of the medium-source Green's function which must be convolved with the distributed source to describe ground motions for large earthquakes.

A proper description of ground motion scaling requires presenting enough information to duplicate the observations. This means that $Q(f)$ cannot be presented without also presenting the $g(r)$ and κ. We must be careful in extrapolating the results to larger earthquakes because we must rely on source estimates from other regions, which means that we must also understand the combination of the $Q(f)$, $g(r)$ and κ used to estimate these other source estimates.

Acknowledgments

this work supported in part by USGS Grants NSF Mid-America Earthquake Center DTRA USGS INGV

References

Akinci, A., L. Malagnini, R. B. Herrmann, N. A. Pino, L. Scognamiglio, and H. Eyidogan (2001). High-frequency ground motion in the Erzincan Region, Turkey: Inferences from small earthquakes *Bull. Seism. Soc. Am.* **91,** 1446-1455.

Anderson, J. G., and S. E. Hough (1984). A model for the shape of the Fourier amplitude spectrum acceleration at high frequencies, *Bull. Seism. Soc. Am.* **74,** 1969-1993.

Anderson J. G., and Y. Lei (1994). Nonparametric description of peak acceleration as a function of magnitude, distance, and site in Guerrero, Mexico, Soc.*Bull.*Seism. **84,** 1003-1017.

Atkinson, G. M., and D. M. Boore (1995). Ground-motion relations for eastern North America, *Bull. Seism. Soc. Am.* **85,** 17-30.

Atkinson, G. M. and R. F. Mereu (1992). The shape of ground motion attenuation in southeastern Canada, *Bull. Seism. Soc. Am.* **82,** 2014-2031.

Atminson, G. M., and W. Silva (1997). An empirical study of earthquake source spectra for California earthquakes, *Bull. Seism. Soc. Am.* **87,** 97-113.

Bay, F., D. Fäh, L. Malagnini and D. Giardini (2003). Spectral shear-wave ground

motion scaling in Switzerland, *Bull. Seism. Soc. Am.* **93,** 414-429.

Boore, D. M. (1983). Stochastic simulation of high-frequency ground motions based on seismological models of the radiated spectrum, *Bull. Seism. Soc. Am.* **73,** 1865-1894.

Boore, D. M. (2003). simulation of ground motion using the stochastic method, *PAGEOPH* **160,** 635-676.

Boore, D. M., and J. Boatwright (1984). Average body-wave radiation coeffi cients, *Bull. Seism. Soc. Am.* **74,** 1516-1621.

Brune, J. N. (1970). Tectonic stress and the spectra of seismic shear waves from earthquakes, *J. Geophys. Res.* **75,** 4997-5009.

Brune, J. N. (1971). Correction, *J. Geophys. Res.* **76,** 5002.

Burger, R., P. Sommerville, J. Barker, R. B. Herrmann and D. Helmberger (1987). the effect of crustal structure on strong ground motion attenuation relations in eastern North America, *Bull. Seism. Soc. Am.* **77,** 420-439.

Cartwright, D. E., and M. S. Longuet-Higgins (1956). The statistical distribution of the maxima of a random function, *Proc. R. Soc. London* **237,** 212-232.

Du, W.-X., W.-Y. Kim and L. R. Sykes (2003). Earthquake source parameters and state of stress for the northeastern United States and southeastern Canada from analysis of regional seismograms, *Bull. Seism. Soc. Am.* **93,** 1633-1648.

Hanks, T. C., and H. Kanamori (1979). A moment magnitude scale, *J. Geophys. Res.* **84,** 2348-2350.

Harmsen, S. (1997). Estimating the diminution of shear-wave amplitude with distance: application to the Los Angeles, California, urban Area *Bull. Seism. Soc. Am.* **87** 888-903.

Herrmann, R. B. (1979). SH-wave generation by dislocation sources - a numerical study, *Bull. Seism. soc. Am.* **69,** 1-15.

Herrmann, R. B. (2003). *Computer Programs in Seismology - 3.25,* Saint Louis University.

Herrmann, R. B., and C. J. Ammon (1997). Faulting parameters of earthquakes in the New Madrid, Missouri region, *Engineering Geology* **46,** 299-311.

Huebner, K. H. (1975). *The finite element method for engineers,* Wiley, New York.

Jeon, Y.-S. (2000). High-frequency earthquake ground motion scaling in Utah, *M. S. Thesis,* Saint Louis University.

Jeon, Y.-S. and R. B. Herrmann (2004). High Frequency Earthquake Ground Motion Scaling in Utah and Yellowstone, *Bull. Seism. Soc. Am.* **94,** (in review).

Malagnini, L., and R. B. Herrmann (2000). Ground motion scaling in the region of the 1997 Umbria-Marche earthquake (Italy), *Bull. Seism. Soc. Am.* **90,** 1041-1051.

Malagnini, L., R. B. Herrmann and M. Di Bona (2000a). Ground motion scaling in the Apennines (Italy), *Bull. Seism. Soc. Am.* **90,** 1062-1081.

Malagnini, L., R. B. Herrmann, and K. Koch (2000b). Ground motion scaling in Germany, *Bull. Seism. Soc. Am.* 1052-1061.

Malagnini, L., A. Akinci, R. B. Herrmann, N. A. Pino and L. Scognamiglio (2002). Characteristics of the ground motion in northeastern Italy, *Bull. Seism. Soc. Am.* **92** 2186-2204.

Ortega, R., R. B. Herrmann and L. Quintinar (2003). High frequency earthquake ground motion scaling in central Mexico between 0.7 and 7 Hz, *Bull. Seism. Soc. Am,* **93**, 397-413.

Raoof, M., R. B. Herrmann and L. Malagnini (1999). Attenuation and Excitation of

Three-Component Ground Motion in Southern California *Bull. Seism. Soc. Am.* **89** 888-902.

Savage, M. K., and J. G. Anderson (1995). A local-magnitude scale for the Western Great Basin - Eastern Sierra Nevada from synthetic Wood-Anderson seismograms, *Bull. Seism. Soc. Am.* **85,** 1236-1243.

Yazd, M. R. S. (1993). Ground motion studies in the southern Great Basin of Nevada and California, *Ph. D. Dissertation*, Saint Louis University.

Department of Earth and Atmospheric Sciences
Saint Louis University
3507 Laclede Avenue
St. Louis, MO 63103, USA
Email: rbh@eas.slu.edu (RBH)

Istituto Nazionale di Geofi sica e Vulcanologia
Via di Vigna Murata, 605, 00143 Rome,Italy
Email: malagnini@ingv.it

FIGURE CAPTIONS

Fig. 1. Fourier acceleration spectra at a distance of 1.0 km from the source. $\beta = 3500\ m/s$ and $\rho = 2.8 kg/m^3$. The constant in (3) is $K = 1.0$

Fig. 2. Epicenters (left) and stations (right) within a 4° x 4° region.

Fig. 3. Shear-wave velocity profiles of the models considered.

Fig. 4. Regression results for Fourier velocity spectra and bandpass filtered peak motions at a frequency of 1.0 Hz for the HCUS model for the SS, MX and 45 sources.

Fig. 5. Comparison of bandpass filtered peak motions for the SS and 45 sources to test sensitivity to crustal thickness. The Moho reflected arrivals, indicated by the arrows for the Z data set, shift to greater distances with increasing crustal thickness.

Fig. 6. Comparison of 1.0 Hz bandpass filtered peak velocities for simple layer-cake model, MCUS, and detailed gradient like model, MHAM. Both models have essentially the same predicted P-wave first arrival times for a surface source and receiver.

Fig. 7. Test of the effect of a thick low velocity sediment section on top of the HCUS model.

Fig. 8. Comparison of simple layered model, HCUS, to an upper crust model with low velocities, NWIT.

Fig. 9. Comparison of $D(r)$ in Fourier and filter time domain velocity as a function of frequency for the HCUS model.

Fig. 10. Comparison of all measured durations, gray cloud, for 45 source for the NWIT and HCUS models at frequencies of 0.25 and 1.0 Hz. The L1 duration estimates as a function of distance are indicated by the dark solid line.

Fig. 11. Peak Fourier and peak filtered velocity excitation (E) at the reference distance of 40 km for the HCUS model and strike-slip mechanism data set with M_W =4.0 for the Z, H and A data sets. The thin black lines are the excitation estimates for the 240 events. The gray curves indicate the predicted levels for moment magnitudes of 3.5 (dashed), 4.0 (solid) and 4.5 (dashed).

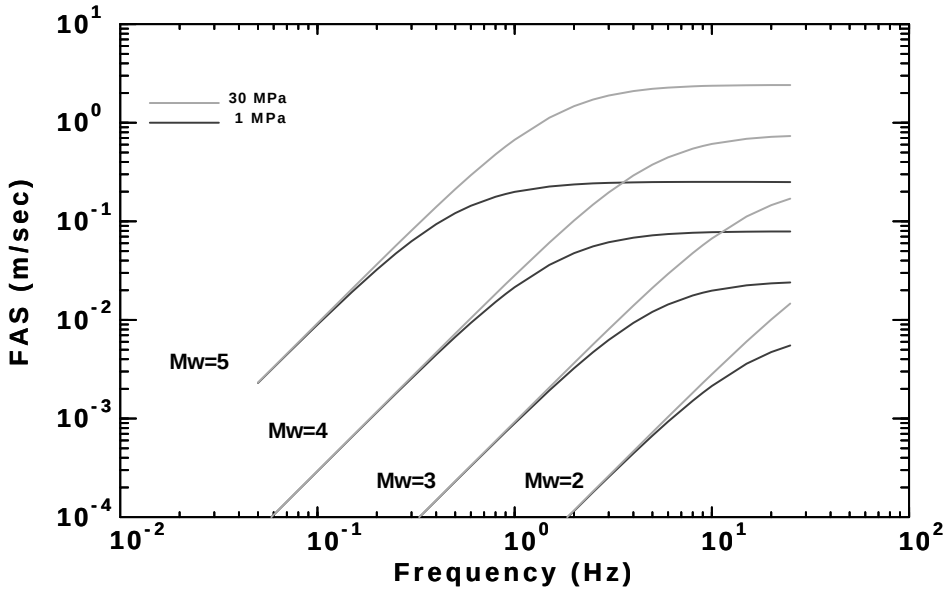

Fig. 1. Fourier acceleration spectra at a distance of 1.0 km from the source. $\beta = 3500\, m/s$ and $\rho = 2.8 kg/m^3$. The constant in (3) is $K = 1.0$

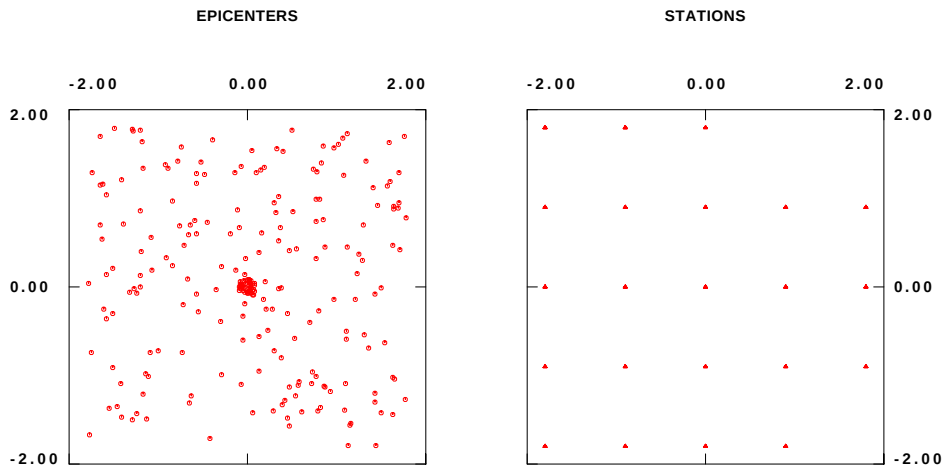

Fig. 2. Epicenters (left) and stations (right) within a 4° x 4° region.

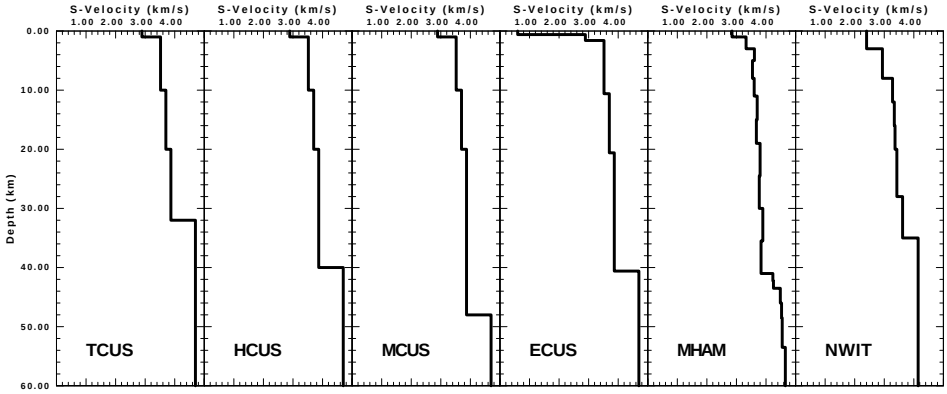

Fig. 3. Shear-wave velocity profiles of the models considered.

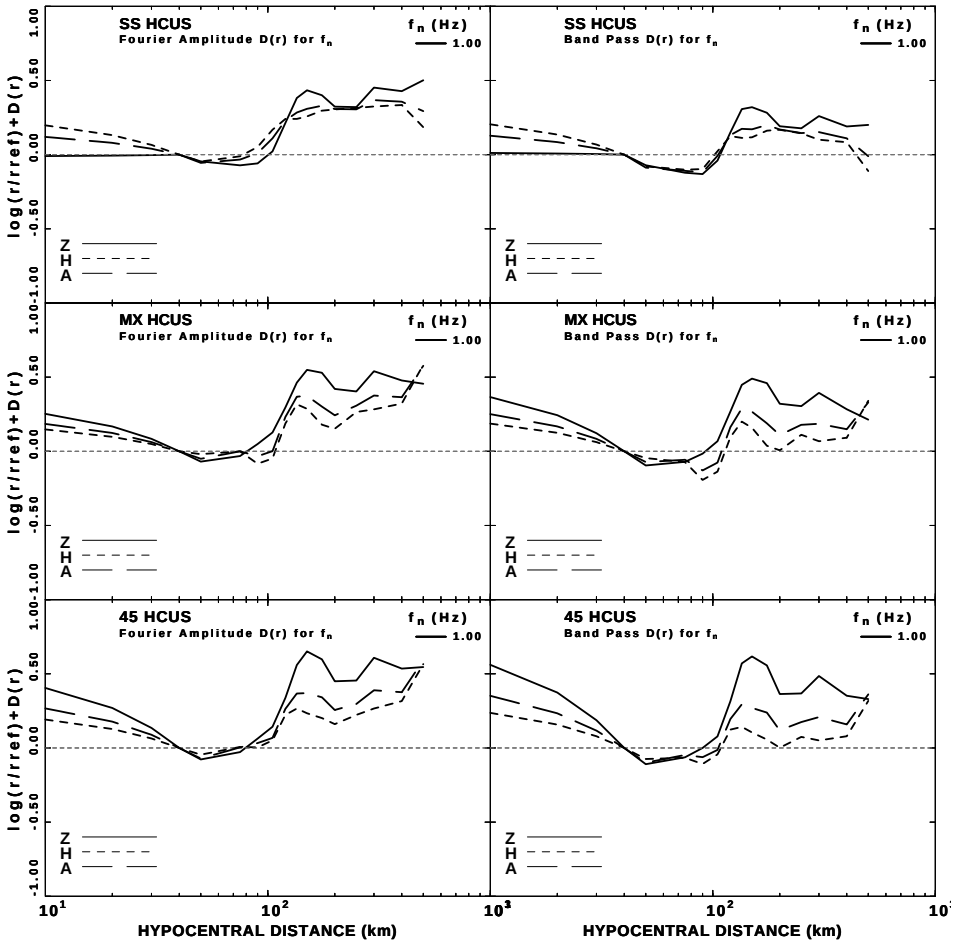

Fig. 4. Regression results for Fourier velocity spectra and bandpass filtered peak motions at a frequency of 1.0 Hz for the HCUS model for the SS, MX and 45 sources.

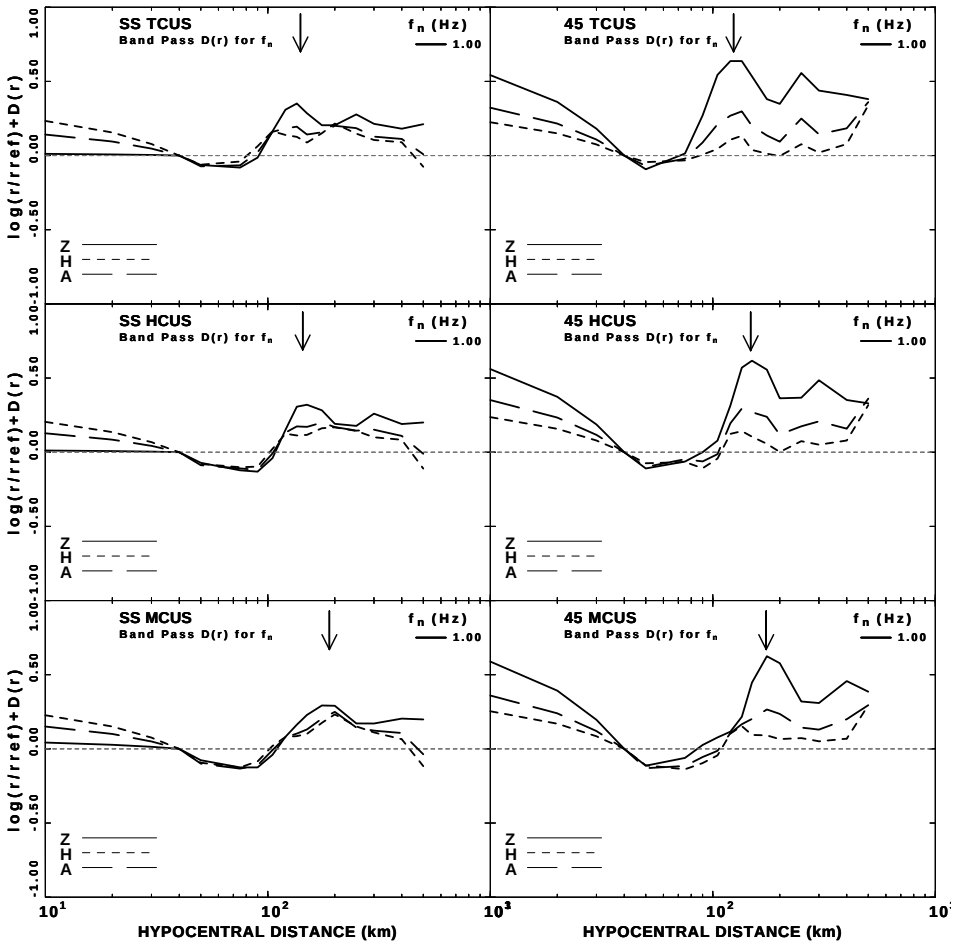

Fig. 5. Comparison of bandpass filtered peak motions for the SS and 45 sources to test sensitivity to crustal thickness. The Moho reflected arrivals, indicated by the arrows for the Z data set, shift to greater distances with increasing crustal thickness.

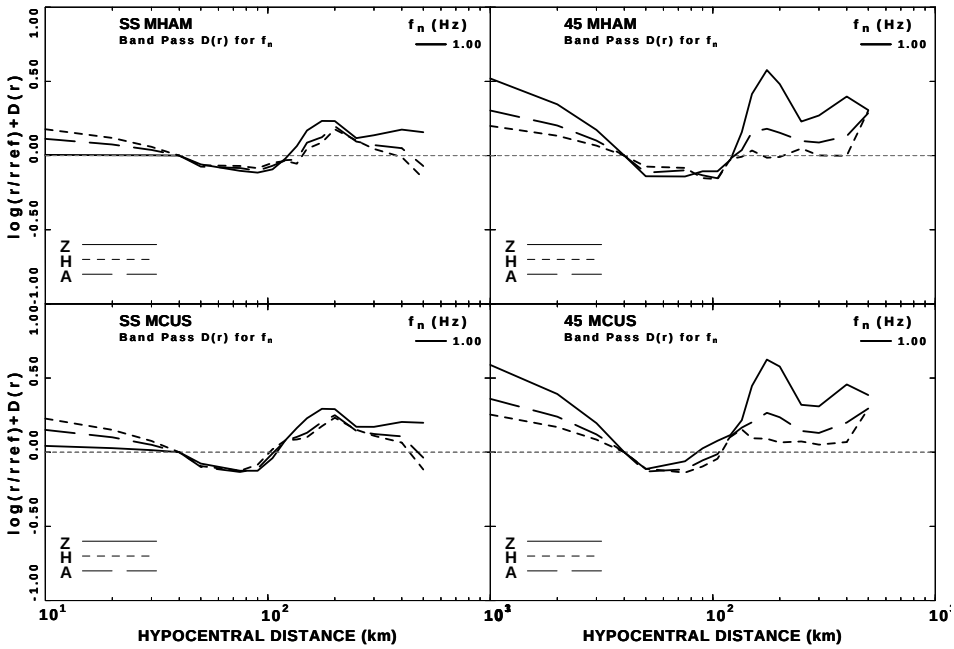

Fig. 6. Comparison of 1.0 Hz bandpass filtered peak velocities for simple layer-cake model, MCUS, and detailed gradient like model, MHAM. Both models have essentially the same predicted P-wave first arrival times for a surface source and receiver.

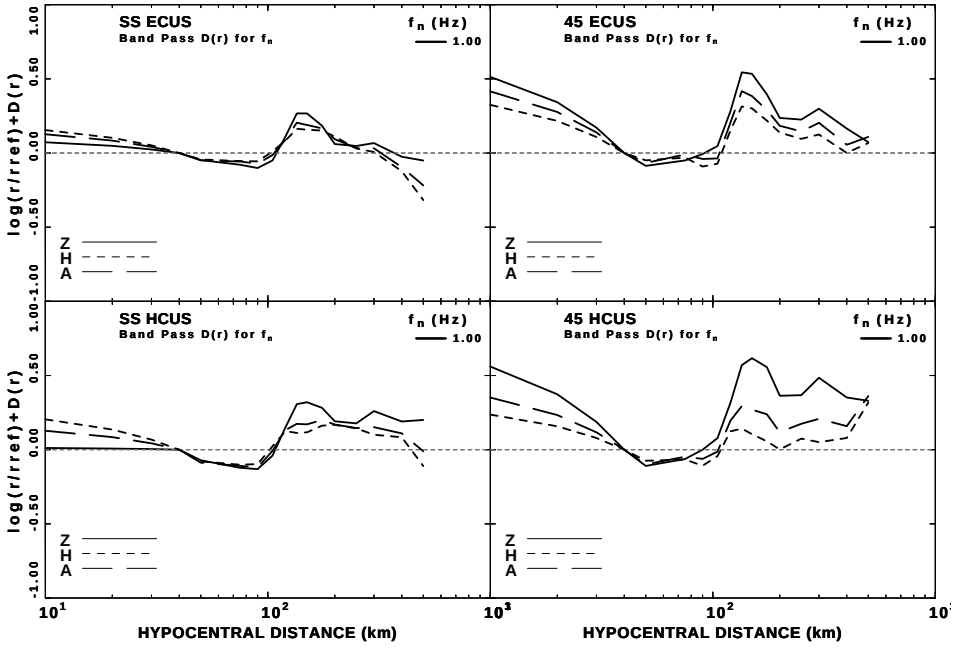

Fig. 7. Test of the effect of a thick low velocity sediment section on top of the HCUS model.

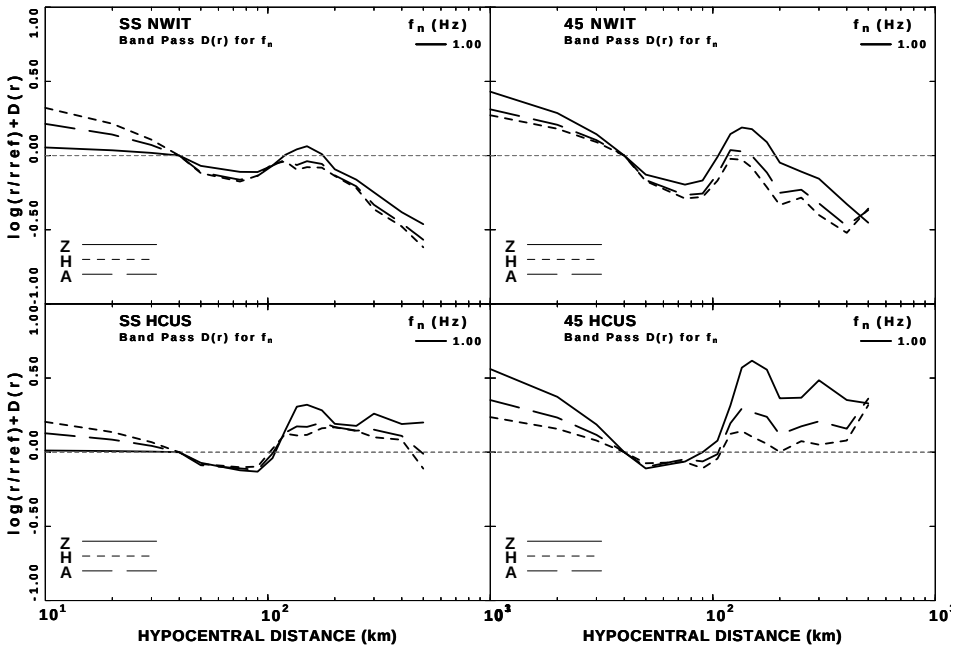

Fig. 8. Comparison of simple layered model, HCUS, to an upper crust model with low velocities, NWIT.

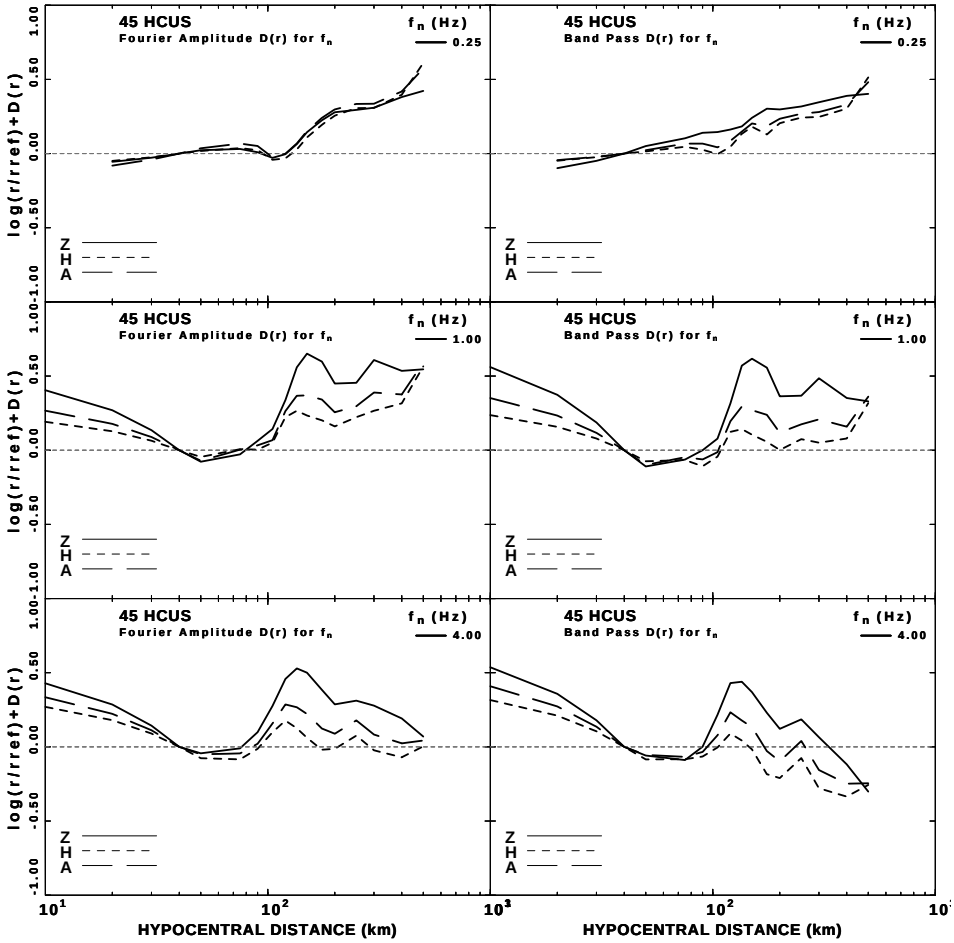

Fig. 9. Comparison of $D(r)$ in Fourier and filter time domain velocity as a function of frequency for the HCUS model.

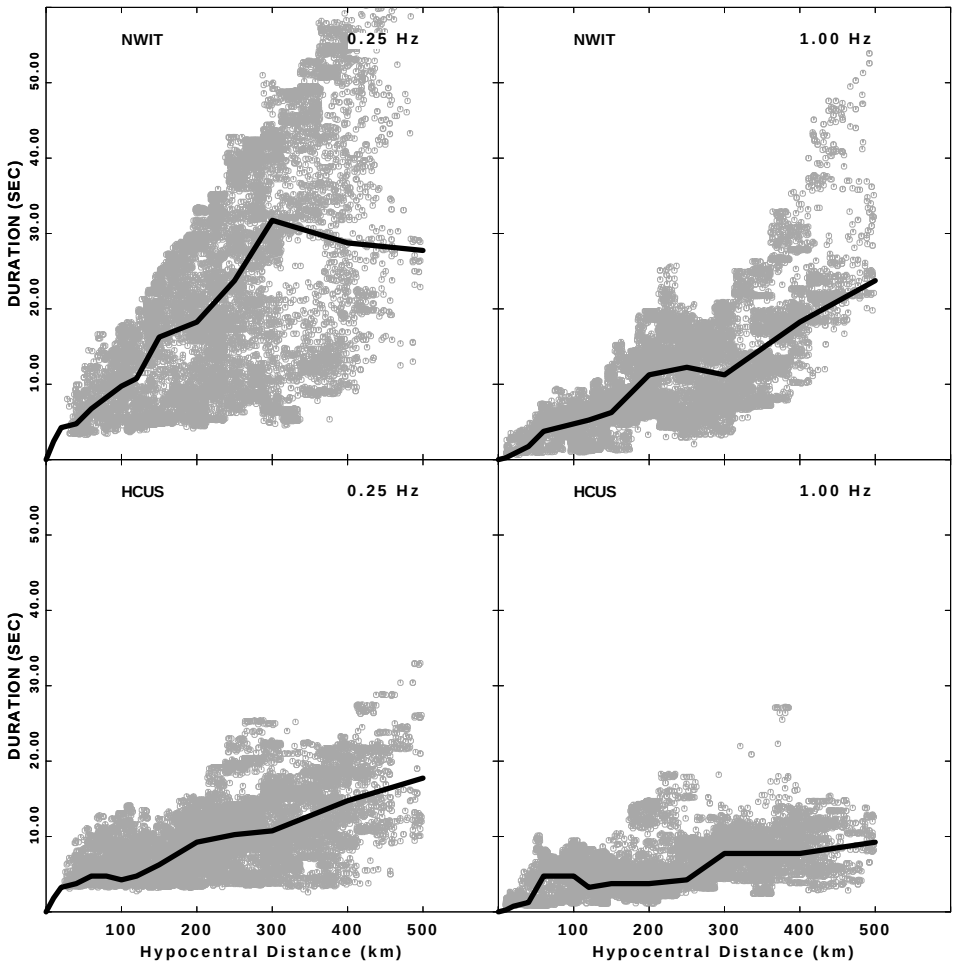

Fig. 10. Comparison of all measured durations, gray cloud, for 45 source for the NWIT and HCUS models at frequencies of 0.25 and 1.0 Hz. The L1 duration estimates as a function of distance are indicated by the dark solid line.

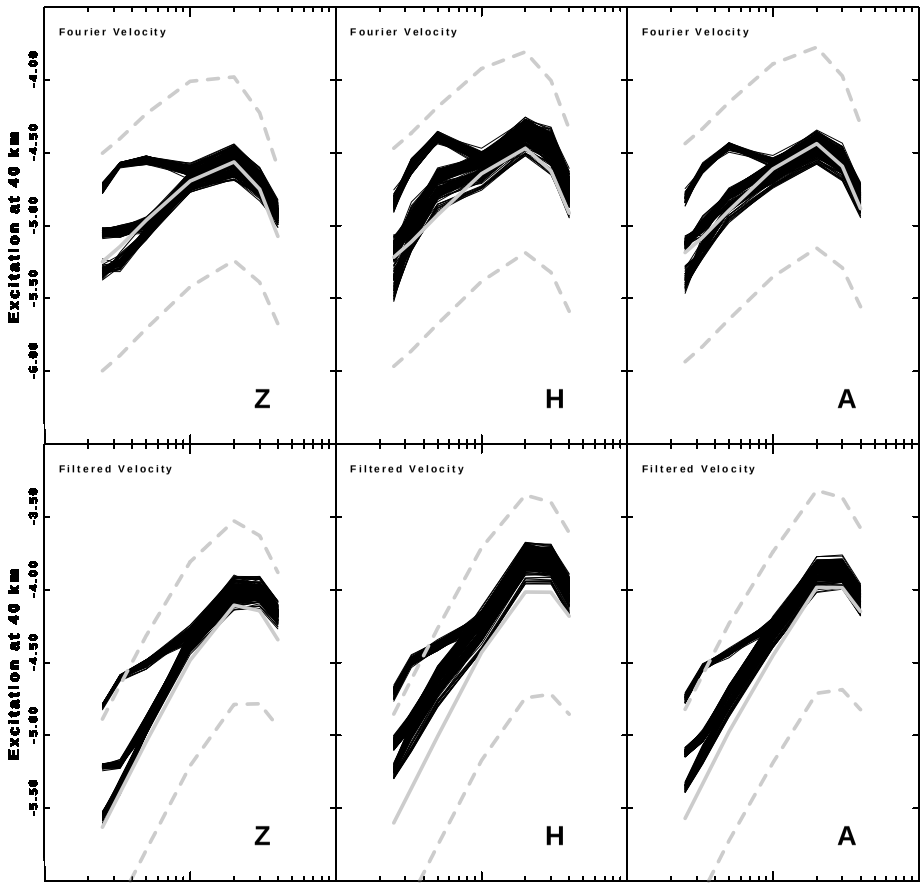

Fig. 11. Peak Fourier and peak filtered velocity excitation (E) at the reference distance of 40 km for the HCUS model and strike-slip mechanism data set with M_W =4.0 for the Z, H and A data sets. The thin black lines are the excitation estimates for the 240 events. The gray curves indicate the predicted levels for moment magnitudes of 3.5 (dashed), 4.0 (solid) and 4.5 (dashed).